



# Structured Surfaces and Morphological Wetting Transitions

REINHARD LIPOWSKY

*MPI für Kolloid- und Grenzflächenforschung, D-14424 Potsdam, Germany*

**Abstract.** Recent theoretical and experimental studies have shown that structured surfaces, which contain patterns of lyophilic surface domains, lead to morphological wetting transitions at which the wetting layer changes its shape in a characteristic and typically abrupt manner. These transitions have been determined for several *specific* surface domain patterns consisting of circular, striped, or ring-shaped domains, as well as for slit pores and slabs bounded by striped surfaces. Such transitions are predicted to be rather generic and to occur for *any* type of structured surface.

**Keywords:** contact angle, surface domains, shape transformations, liquid microchannels

## 1. Introduction

The structured surfaces considered here consist of two types of surface domains denoted by  $\gamma$  and  $\delta$ . These domains may form a variety of patterns as shown in Fig. 1. The basic length scale of such a surface domain pattern is provided by the linear size  $L_\gamma$  of the  $\gamma$  domains. The spatial region above the structured substrate is filled with a fluid phase denoted by  $\alpha$ . In addition, this region contains a certain amount of another liquid,  $\beta$ , which wants to maximize its contact area with the  $\gamma$  domains but tries to avoid the  $\delta$  domains. Thus, the  $\gamma$  and  $\delta$  domains are lyophilic and lyophobic, respectively, with respect to the  $\beta$  phase.

When a certain volume  $V_\beta$  of the  $\beta$  phase is placed onto the structured surface, it will form a wetting layer which tries to maximize and minimize the contact with the lyophilic  $\gamma$  and the lyophobic  $\delta$  domains, respectively. At the same time, the wetting layer will also try to attain a state for which the area of the  $\alpha\beta$  interface is as small as possible. These two contributions to the free energy compete and lead, in general, to a morphological wetting transition at a certain volume  $V_\beta = V_c$  of the  $\beta$  phase at which the shape of the wetting layer changes in a characteristic and typically abrupt manner [1–3].

This article is organized as follows. First, Section 2 contains a brief review of the various experimental methods, by which one may construct structured sur-

faces, and describes three different types of experiments, for which the volume  $V_\beta$  of the  $\beta$  phase can be varied in a controlled way. The systematic theoretical framework based on effective interface models is described in Section 3. One new aspect which is emphasized in this section is that each pattern of lyophilic  $\gamma$  domains can be characterized by a unique volume  $V_\gamma$ . Section 4 discusses several types of surface domain patterns and the corresponding wetting morphologies: a droplet on a single surface domain, an ensemble of droplets on several surface domains, channels and channel transitions, as well as bridges between structured surfaces. The final chapter contains a brief summary and an outlook.

## 2. Structured Surfaces and Wetting Layers

### 2.1. Construction of Surface Domains

A variety of experimental methods is available by which one can create surface patterns with domain sizes  $L_\gamma$  in the milli-, micro-, and nanometer range. In the millimeter range, one may use screen printing technology in order to print hydrophobic coatings on glass surfaces [4] or printed circuit board technology in order to create lyophilic domains for molten tin-lead alloys as used in soldering processes [5].

Several methods have been used to create structured surfaces with surface domains in the micrometer

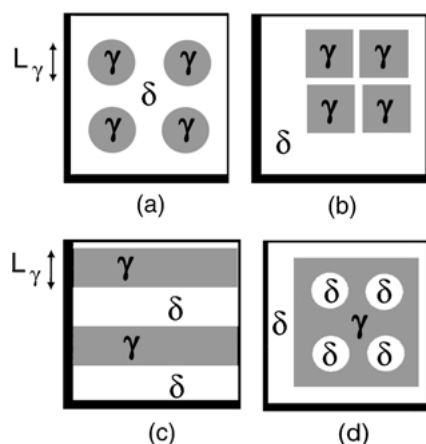


Figure 1. Top view of structured surfaces which contain lyophilic  $\gamma$  domains (grey) within a lyophobic matrix  $\delta$  (white): (a) A regular pattern of circular  $\gamma$  domains; (b) A regular pattern of quadratic  $\gamma$  domains; (c) A pattern consisting of  $\gamma$  stripes; and (d) A large quadratic  $\gamma$  domain containing smaller  $\delta$  domains. The domain size of the  $\gamma$  domains is denoted by  $L_\gamma$ .

range: (i) Elastomer stamps by which one can create patterns of hydrophobic alkanethiol on metal surfaces [6–9]; (ii) Vapor deposition through grids which cover part of the surface [10]; (iii) Photolithography of amphiphilic monolayers which contain photosensitive molecular groups [11]; (iv) Domain formation in Langmuir-Blodgett monolayers transferred to solid substrates [12]; (v) Unstable monolayers produced by such monolayer transfer [13]; (v) Electrophoretic assembly of colloids [14] or (v) Anisotropic rupture of polymer films on top of a polymeric surface [15].

Furthermore, new experimental methods are being developed in order to construct patterns with even smaller domain sizes in the nanometer range. These methods include lithography with colloid monolayers [16], atomic beams modulated by light masks [17], microphase separation in diblock copolymer films [18], or local oxidation of silicon surfaces induced by atomic force microscopy [19].

## 2.2. Volume as Control Parameter

Now, consider such a structured surface in contact with the bulk phase  $\alpha$ , and let us place a certain amount of  $\beta$  phase on top of this surface. In general, the  $\alpha$  and the  $\beta$  phase may represent any type of material and, thus, can be fluid or solid. In order to be specific, we will focus on the situation in which the  $\beta$  phase is a liquid and the  $\alpha$  phase is a vapor or another liquid.

After the  $\beta$  phase has been deposited on the structured surface, it will form a wetting layer which tries to maximize its contact area with the lyophilic  $\gamma$  domains, and, at the same time, to minimize the total area of its  $\alpha\beta$  interface. Depending on the shape and the pattern of these surface domains, the  $\beta$  phase may form a variety of different wetting structures: a single drop, which can have a nonspherical shape, a pattern of disconnected droplets, a perforated or continuous wetting layer or even bridges between disconnected domains within the substrate surface.

As mentioned in the introduction, the volume  $V_\beta$  of the  $\beta$  phase plays the role of a control parameter. This parameter can be varied systematically in three types of experiments which correspond to three different types of equilibrium between the  $\alpha$  and the  $\beta$  phase:

- (i) The  $\beta$  phase is a nonvolatile liquid and the exchange of molecules between the  $\alpha$  and the  $\beta$  phase can be ignored on the relevant time scales. In this case, the volume of the  $\beta$  phase is fixed and does not change during the wetting process. If one droplet of  $\beta$  phase is placed on a *single* lyophilic  $\gamma$  domain, it will try to spread over the whole domain. The final state will usually correspond to a state of minimal free energy. The situation is somewhat more complex if the initial  $\beta$  drop is large and covers *several disconnected*  $\gamma$  domains. In such a situation, the state of minimal free energy may correspond to an ensemble of several  $\beta$  droplets, but the  $\beta$  phase may not be able to attain this state since it involves a change in its topology. In other words, the rupture of the initial  $\beta$  drop into several  $\beta$  droplets may represent a relatively large activation barrier which prevents the  $\beta$  phase from attaining its state of minimal free energy. In such a situation, the wetting morphology represents a state which is only locally stable or metastable.
- (ii) The  $\beta$  phase is a volatile liquid which condenses from a supersaturated vapor or liquid mixture  $\alpha$  onto the  $\gamma$  domains. Indeed, the activation barriers for surface nucleation at the  $\gamma$  domains vanish for small contact angle  $\theta = \theta_\gamma$ , and, thus, can be much smaller than the activation barriers for homogeneous nucleation in the bulk  $\alpha$  phase. The  $\beta$  phase will then start to condense on these domains even though the bulk phase  $\alpha$  does not decay and remains in its metastable state. In this case, the total amount of  $\beta$  phase increases with time, but if this growth process is slow, the resulting time

evolution of the droplet morphology will correspond to a sequence of equilibrium states. These latter states have minimal free energy for a given volume of condensed  $\beta$  phase; and

- (iii) The  $\beta$  phase is a volatile liquid which is in thermal and chemical equilibrium with the  $\alpha$  phase. In this case, the total amount of  $\beta$  phase is determined by the total volume of the system and by the total number of particles according to the usual Gibbs rules.

### 3. Effective Interface Models

The different morphologies of the wetting layer can be distinguished by the shape of the two types of interfaces bounding the  $\beta$  phase: (i) the  $\alpha\beta$  interface which represents the contact region between the  $\beta$  and the  $\alpha$  phase, and (ii) the  $\beta\sigma$  interface which separates the  $\beta$  phase from the structured substrate  $\sigma$ . The shape of the  $\beta\sigma$  interface is taken to be fixed corresponding to a rigid and inert substrate. The shape of the  $\alpha\beta$  interface, on the other hand, is flexible and can adapt to the underlying pattern of surface domains.

From the theoretical point of view, the shape of the  $\alpha\beta$  interface is determined by the free energy of the wetting layer. This free energy contains three different contributions: the first contribution is proportional to the volume of the  $\beta$  phase, the second to the area of the  $\alpha\beta$  and the  $\beta\sigma$  interfaces, and the third to the length of the contact line which represents the line of intersection between the  $\alpha\beta$  interface and the structured surface.

#### 3.1. Free Energy Contributions

The volume contribution to the free energy of the wetting layer depends on the difference  $\Delta P \equiv P_\alpha - P_\beta$  between the pressures in the  $\alpha$  and  $\beta$  phases. For a given volume  $V_\beta$  of  $\beta$  phase, the pressure difference  $\Delta P$  plays the role of a Lagrange multiplier which is conjugate to the prescribed volume. If the  $\alpha$  and  $\beta$  phases are in thermal and chemical equilibrium, this pressure difference is related to the chemical potentials of the molecules. In the simplest case, one has only one molecular species and, thus, only one chemical potential  $\mu = \mu(T, P)$  which has two branches  $\mu = \mu_\alpha(T, P)$  and  $\mu = \mu_\beta(T, P)$ . The pressure difference is then given by

$$\Delta P = P_\alpha - P_\beta \approx [N_\alpha - N_\beta][\mu_\beta(T, P_\beta) - \mu_\beta(T, P_0)] \quad (1)$$

where  $P_o = P_o(T)$  represents the pressure at  $\alpha\beta$  coexistence and  $N_\alpha$  and  $N_\beta$  are the particle number densities of the two coexisting phases.

In addition to the pressure term, the volume free energy may depend on body forces such as gravity. In the following, these terms will not be discussed explicitly even though one may easily incorporate them into the theoretical description, see, e.g., [20]. In practise, gravity becomes important as soon as the height of the wetting layer exceeds the so-called capillary length

$$L_{\text{cap}} \equiv [2\Sigma_{\alpha\beta}/g\Delta\rho]^{1/2} \quad (2)$$

of the liquid where  $\Sigma_{\alpha\beta}$  is the interfacial tension of the  $\alpha\beta$  interface,  $\Delta\rho$  the difference in mass density between the  $\alpha$  and the  $\beta$  phase, and the gravitational acceleration  $g = 9.81 \text{ m/s}^2$ . For water at room temperature, one has  $\Sigma_{\alpha\beta} \simeq 72 \text{ mJ/m}^2$  and  $\Delta\rho \simeq 10^3 \text{ kg/m}^3$  which leads to  $L_{\text{cap}} \simeq 3.8 \text{ mm}$ . Large droplets sitting on a horizontal surface are flattened out by gravity (which acts perpendicular to this surface) if their height exceeds  $L_{\text{cap}}$ ; they then assume the shape of a flat ‘pancake’ with a thickness of the order of  $L_{\text{cap}}$ .

The second contribution to the free energy arises from the interfacial tensions  $\Sigma_{\alpha\beta}$  and  $\Sigma_{\beta\sigma}$  of the  $\alpha\beta$  and the  $\beta\sigma$  interface, respectively. Each of these two contributions is proportional to the corresponding interfacial area. In general, the  $\beta$  phase may consist of several disconnected pieces which implies several disconnected segments of the  $\alpha\beta$  and the  $\beta\sigma$  interface.

The  $\alpha\beta$  interface, which separates two fluid phases, is laterally homogeneous and thus characterized by uniform interfacial tension  $\Sigma_{\alpha\beta}$ . The  $\beta\sigma$  interface, on the other hand, lies within the structured surface, which is taken to be rigid and inert, but may have a chemically nonuniform composition. This leads to position-dependent tensions  $\Sigma_{\beta\sigma} = \Sigma_{\beta\sigma}(\mathbf{x})$  and  $\Sigma_{\alpha\sigma} = \Sigma_{\alpha\sigma}(\mathbf{x})$  where  $\mathbf{x} \equiv (x_1, x_2)$  represents the surface coordinate of the  $\sigma$  substrate.

Finally, the contact line, which may again consist of several disconnected segments, contributes a free energy term which is proportional to its total length. The corresponding line tension will be denoted by  $\Lambda$ . In general, this quantity can be positive or negative [21], and may also depend on the surface coordinate  $\mathbf{x}$  [3, 22].

#### 3.2. Equilibrium Shapes of Constant Mean Curvature

As explained in the previous subsection, we will focus on wetting layers in the submillimeter regime for which

the effects of gravity can be ignored. Minimization of the total free energy then leads to the classical Laplace equation and to a general Young equation. The Laplace equation is given by

$$2M\Sigma_{\alpha\beta} = P_\beta - P_\alpha = -\Delta P \quad (3)$$

which determines the mean curvature  $M$  of the  $(\alpha\beta)$  interface.

In general, each point  $\mathbf{r}_l$  within the interface is characterized by the mean curvature  $M(\mathbf{r}_l) \equiv [C_1(\mathbf{r}_l) + C_2(\mathbf{r}_l)]/2$  where  $C_1$  and  $C_2$  are the two principal curvatures which are equal to the inverse curvature radii. These two principal curvatures can be found as follows. First, construct the unit vector  $\hat{N}$  normal to the interface at the point  $\mathbf{r}_l$ . Next, consider a normal plane through the point  $\mathbf{r}_l$  parallel to the normal vector  $\hat{N}$ . The contour of the interface within this normal plane, the so-called normal section, represents a planar curve for which one may easily determine the curvature  $C$  at point  $\mathbf{r}_l$ . As one rotates the normal plane around the normal vector, the normal section and its curvature  $C$  at  $\mathbf{r}_l$  will, in general, change. The two principal curvatures  $C_1$  and  $C_2$  correspond to the minimal and the maximal values of the curvature  $C$  of the normal section, respectively. In more abstract terms, the two principal curvatures  $C_1$  and  $C_2$  represent the eigenvalues of the second fundamental form of the surface, and  $2M = C_1 + C_2$  is equal to the trace of this form. This implies that  $M$  is invariant under arbitrary reparametrizations of the surface.

The Laplace Eq. (3) has the remarkable consequence that the mean curvature  $M$  has the same value for all points within the  $\alpha\beta$  interface. This follows from (3) since both the interfacial tension  $\Sigma_{\alpha\beta}$  and the pressure difference  $P_\beta - P_\alpha$  are uniform for a fluid–fluid interface. Note that the sign of  $M$  is opposite to the sign of  $\Delta P$  since the interfacial tension  $\Sigma_{\alpha\beta} > 0$ . Furthermore, the definition of  $M$  involves a sign convention which is chosen in such a way that a spherical cap has positive mean curvature  $M > 0$ .

The second equation obtained from the minimization of the total free energy determines the contact angles along the contact line. This generalized or modified Young equation has the form [22]

$$\Sigma_{\alpha\beta} \cos(\theta(\mathbf{x})) = \Sigma_{\alpha\sigma}(\mathbf{x}) - \Sigma_{\beta\sigma}(\mathbf{x}) - \Lambda(\mathbf{x})C_{\alpha\beta\sigma} - \hat{n} \cdot \nabla_x \Lambda(\mathbf{x}) \quad (4)$$

where the variable  $C_{\alpha\beta\sigma}$  is the curvature of the contact line and  $\hat{n}$  is the unit normal vector which is perpendicular both to the contact line and to the surface normal

$\hat{N}$  at this line. The symbol  $\nabla_x$  is the 2–dimensional gradient with respect to the coordinate  $\mathbf{x}$  of the substrate surface.

For contact lines which lie within a planar substrate, the two line tension terms in (4) can be combined which leads to

$$\Sigma_{\alpha\beta} \cos[\theta(\mathbf{x})] = \Sigma_{\alpha\sigma}(\mathbf{x}) - \Sigma_{\beta\sigma}(\mathbf{x}) - \nabla_x \cdot (\hat{n} \Lambda(\mathbf{x})) \quad (5)$$

If line tension can be ignored, the modified Young equation has the same functional form as the usual Young equation but with  $\mathbf{x}$ -dependent interfacial tensions  $\Sigma_{\alpha\sigma}$  and  $\Sigma_{\beta\sigma}$  [1]. Special cases of the line tension terms have been previously derived for planar and homogeneous surfaces [23], for surface heterogeneities which are axially symmetric [24] and for heterogeneities which are translationally invariant with respect to one surface coordinate [25]. The general form of the line tension term as given by (4) and (5) was first obtained in [22].

### 3.3. Reference Volume for Surface Domain Pattern

As emphasized, it follows from the Laplace Eq. (3) that the stable and metastable states of the wetting layer are characterized by shapes of *constant mean curvature*. A similar shape problem is encountered (i) for soap bubbles [26] and (ii) for the surface of fluids which protrude from several orifices of a tube [27]. From a mathematical point of view, the main difference between the shape of bubbles and the wetting morphologies considered here arises from the constraints which the underlying pattern of surface domains imposes onto the position of the contact line via the generalized Young Eq. (4).

The precise position of the contact line is, in general, difficult to calculate. However, it is very instructive to consider the limiting case in which this line is pinned to the  $\gamma\delta$  domain boundaries within the structured surface, which implies that the contact area between the  $\beta$  phase and the structured substrate surface is equal to the area of the  $\gamma$  domains. One then has to calculate shapes of constant mean curvature  $M$  with prescribed boundaries. For this problem, several mathematical theorems are available which ensure (i) The existence of a constant  $M$  surface as long as  $M$  is sufficiently small, (ii) The nonexistence of such a surface if  $M$  is sufficiently large, and (iii) The existence of two different shapes with the same  $M$ , known as the ‘small’ and the ‘large’ solution, for an intermediate range of  $M$  values [28–32].

If one ignores exceptional cases, these theorems imply that, for any prescribed position of the contact line, there exists a shape of *maximal* mean curvature  $M = M_{\max}$ . Therefore, if one considers the situation in which the contact line is pinned to the  $\gamma\delta$  domain boundaries, any pattern of surface domains can be characterized by a unique constant mean curvature shape with  $M = M_{\max}$ . The volume of this latter shape provides a *unique reference volume*  $V = V_\gamma$ . Morphological wetting transitions occur if the volume  $V_\beta$  of the  $\beta$  phase is of the same order of magnitude as  $V_\gamma$ .

It is instructive to discuss some examples. First, consider the pattern of circular domains as shown in Fig. 1(a). In this case, the maximal mean curvature shapes consist of *half spheres* which have the same diameter  $L_\gamma$  as the circular domains. Thus, the reference volume  $V_\gamma$  is equal to  $V_\gamma = N(\pi/12)L_\gamma^3$  where  $N$  denotes the number of domains. For the long  $\gamma$  stripes shown in Fig. 1(c), the maximal mean curvature shapes are *half cylinders* the diameter of which is equal to the width  $L_\gamma$  of the stripes. Finally, for ring-shaped domains as studied in Ref. [5], the maximal mean curvature shape is provided by nodoids.

### 3.4. Interfacial Versus Line Tensions

The relative magnitude of the free energy contributions arising from the interfaces and from the contact line can be estimated by dimensional analysis. As mentioned, the contribution from the contact line is governed by the line tension  $\Lambda$ . For a wetting layer with linear dimension  $L_\beta$ , this free energy contribution is of the order of  $L_\beta\Lambda$ . The interfacial free energies, on the other hand, are of the order of  $L_\beta^2\Sigma_{\alpha\beta}$  which depends on the tension  $\Sigma_{\alpha\beta}$  of the  $\alpha\beta$  interface. These two contributions are comparable if the linear dimension  $L_\beta$  of the wetting layer is of the order of the characteristic length scale [3]

$$L_\beta^* \equiv |\Lambda|/\Sigma_{\alpha\beta}. \quad (6)$$

Therefore, for  $L_\beta \gg L_\beta^*$ , one can safely ignore the free energy contributions arising from the tension of the contact line.

The magnitude of  $L_\beta^*$  can be estimated from the experimentally observed values of  $\Sigma_{\alpha\beta}$  and  $\Lambda$ . The interfacial tension  $\Sigma_{\alpha\beta}$  can be measured by a variety of experimental methods; for water at room temperature, one finds  $\Sigma_{\alpha\beta} \simeq 72 \text{ mJ/m}^2$  as mentioned. A rough estimate for this interfacial tension can be obtained from  $\Sigma_{\alpha\beta} \simeq T/\ell_{\text{mol}}^2$  where  $T$  is the temperature in energy units and  $\ell_{\text{mol}}$  represents a molecular length scale. For

$\ell_{\text{mol}} \simeq 0.3 \text{ nm}$  and room temperature, this leads to  $\Sigma_{\alpha\beta} \simeq 50 \text{ mJ/m}^2$ , i.e., to the correct order of magnitude. Exceptionally small values for the interfacial tension are observed close to a bulk critical point at which the  $\alpha$  and the  $\beta$  phase become identical.

The line tension  $\Lambda$  is more difficult to measure. In fact, the numerical values for  $\Lambda$ , which have been deduced experimentally, vary over a wide range as given by  $10^{-11} \text{ J/m} \lesssim |\Lambda| \lesssim 10^{-6} \text{ J/m}$  [33–36]. In order to obtain an intuitive understanding of this variation, it is instructive to define an effective width  $\ell_{\alpha\beta\sigma}$  of the contact line via  $|\Lambda| \equiv (T/\ell_{\text{mol}}^3)\ell_{\alpha\beta\sigma}^2$ . [3] The observed range of  $|\Lambda|$  values then corresponds to the range  $1 \lesssim \ell_{\alpha\beta\sigma}/\ell_{\text{mol}} \lesssim 300$  for the effective width of the contact line. These different values for  $\ell_{\alpha\beta\sigma}$  presumably reflect different types of small scale heterogeneities which were present on the different substrate surfaces used in the experiments.

As a typical example, consider an  $\alpha\beta$  interface characterized by  $\Sigma_{\alpha\beta} \simeq 72 \text{ mJ/m}^2$  as appropriate for water and a line tension  $|\Lambda|$  of the order of  $10^{-9} \text{ J/m}$  corresponding to an effective contact line width  $\ell_{\alpha\beta\sigma} \simeq 3 \text{ nm}$ . In this case, the characteristic size  $L_\beta^*$  as given by (6) is  $\simeq 30 \text{ nm}$ , and contributions from the contact line play no role for wetting layers with linear dimensions in the micrometer regime.

### 3.5. Separation of Length Scales

The theoretical approach described above is rather robust since it depends only on a small number of parameters. Indeed, for a wide range of domains sizes  $L_\gamma$  with  $L_\beta^* \lesssim L_\gamma \lesssim L_{\text{cap}}$ , the only relevant parameters are the interfacial tensions (or the corresponding contact angles). As explained in more detail below, this approach has been used in order to determine the parameter dependence of the wetting layer morphologies for a variety of surface domain patterns consisting of circular domains [1], striped domains [2, 37], and ring-shaped domains [5], as well as for slit pores or slabs with striped surfaces [38, 39].

As one considers smaller surface domains with linear dimensions  $L_\gamma$  of the order of  $L_\beta^*$ , one should also include the line tension terms. Since the contact line sits directly on the substrate surface, its structure and its tension will be sensitive to the local topography and to the local composition of this surface. Thus, as one studies smaller and smaller domain sizes  $L_\gamma$  and looks at smaller and smaller wetting structures, additional length scales, which are related to the molecular

structure of the substrate surface, will start to affect the wetting behavior.

A particularly simple example is provided by very thin wetting layers on substrate surfaces with an idealized topography. If the wetting layer thickness  $\ell$  is in the nanometer range, the layer experiences a body potential arising from the molecular interactions with the substrate. These interactions lead to an  $\ell$ -dependent layer free energy. The corresponding disjoining pressure was first studied by the Derjaguin school [40] and can be calculated using the methods of statistical mechanics. For wetting of homogeneous and planar surfaces, such calculations have been performed both for short-ranged [41, 42], and for long-ranged forces [43–45]. More recently, this approach has been extended to structured surfaces using variational methods [46–52] and computer simulations [53, 54].

On the molecular scale, the contact line corresponds to the spatial region between a very thin wetting layer close to the substrate surface, which is governed by the molecular interactions with this surface, and more distant segments of the  $\alpha\beta$  interface, which do not experience such interactions from the substrate. Therefore, the effective width of the contact line will, in general, depend on various molecular length scales such as (i) The width of the  $\gamma\delta$  domain boundaries; (ii) Additional length scales related to quenched or frozen undulations of these domain boundaries which increase the curvature of these domain boundaries and can lead to folds of the  $\alpha\beta$  interface emanating from the contact line [3]; (iii) The correlation length for composition fluctuations within a given surface domain which are taken into account by the Cassie equation [22, 55, 56]; (iv) The topographical roughness of the structured surface; and (v) The intrinsic width of the  $\alpha\beta$  interface.

In the following, these various molecular length scales, which may all contribute to the effective contact line width, are assumed to be small compared to the linear size  $L_\gamma$  of the surface domains. These molecular scales are then irrelevant for the wetting layer morphology and may be safely ignored in the theoretical description.

## 4. Different Wetting Morphologies

### 4.1. Droplet on a Single Surface Domain

As a simple example, consider a single lyophilic  $\gamma$  domain which has a circular shape embedded in a lyophobic  $\delta$  matrix. If we place a small amount of liquid onto

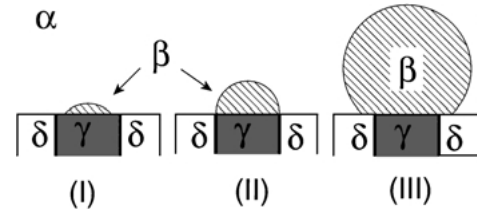


Figure 2. Droplet on single lyophilic  $\gamma$  domain in a lyophobic  $\delta$  matrix: Depending on the droplet volume, the droplet state belongs to regime (I) with contact angle  $\theta = \theta_\gamma$ , to regime (III) with  $\theta = \theta_\delta$ , or to the intermediate regime (II) in which the contact angle can freely adapt its value within the range  $\theta_\gamma < \theta < \theta_\delta$ .

this domain, it forms a spherical cap with contact angle  $\theta_\gamma$ . As we add more liquid to this droplet, it grows until it covers the whole  $\gamma$  domain. At this point, the contact line sits on top of the surface domain boundary  $\gamma\delta$ . If we continue to add liquid, the contact area of the droplet remains fixed while the contact angle grows until it reaches the value  $\theta_\delta$ . Beyond this point, the droplet starts to increase its contact area and to spread onto the lyophobic matrix where it attains the contact angle  $\theta_\delta$ .

Thus, one must distinguish three different droplet regimes (I)–(III), as indicated in Fig. 2. Regime (I) corresponds to sufficiently small droplets which are located within the  $\gamma$  domain and have contact angle  $\theta_\gamma$ . Regime (III) is given by sufficiently large droplets which have spread onto the lyophobic matrix and have contact angle  $\theta_\delta$ . For intermediate volumes, one encounters the droplet regime (II). In this latter regime, the contact angle does *not* satisfy the Young equation. Instead, the contact angle now fulfills the inequalities [1]

$$\theta_\gamma \leq \theta \leq \theta_\delta \quad \text{for regime (II)}. \quad (7)$$

In this regime, the contact line is pinned to the circular domain boundary and the  $\alpha\beta$  interface forms a spherical cap. The latter shape is a simple example of a constant mean curvature surface with a prescribed boundary. It is not difficult to realize that the mean curvature  $M$  is not monotonic with increasing droplet volume but reaches a maximum value as the droplet attains the shape of a half sphere, i.e., as the contact angle attains the value  $\theta = \pi/2$ . Thus, in this simple example, the reference volume  $V_\gamma$  defined in Section 3.3 has the value  $V_\gamma = (\pi/12)L_\gamma^3$  corresponding to a half sphere of diameter  $L_\gamma$ .

For a circular domain boundary, it is difficult to envisage a shape which has a lower free energy than a

spherical cap (in the absence of body forces as considered here). For regime (I) and regime (III), these caps correspond to the usual droplet shapes for homogeneous  $\gamma$  and  $\delta$  surfaces, respectively. In regime (II), on the other hand, any shape for which the contact line is partially pinned to and partially detached from the circular domain boundary will induce some folds along the interface and, thus, should have a larger free energy.

The situation becomes more complex, however, if the surface domain has a non-circular shape. In this case, the contact line may consist of different segments which are attached and detached from the  $\gamma\delta$  domain boundary, respectively. One example is provided by a channel on a striped  $\gamma$  domain which develops a bulge, see Section 4.3 below. If the contact angle  $\theta_\gamma$  of the lyophilic stripe is sufficiently small and the stripe is sufficiently long, the bulge state of the channel is characterized by a contact line which detaches itself partially from the boundary of the lyophilic  $\gamma$  domain and makes an excursion across the lyophobic  $\delta$  matrix.

It is instructive to consider the limiting case of strongly lyophilic and strongly lyophobic surface domains with  $\theta_\gamma = 0$  and  $\theta_\delta = \pi$ , respectively. In this situation, the  $\alpha\beta$  interface of the droplet is a constant mean curvature surface with  $M > 0$ , and the contact line cannot stay within the lyophilic  $\gamma$  domain [39]. Thus, there is no regime (I) and the contact line is pinned to the  $\gamma\delta$  domain boundary for small and intermediate volumes  $V_\beta$  irrespective of the shape of the  $\gamma\delta$  domain boundary. For large volumes, on the other hand, the contact line may detach partially from this domain boundary and make an excursion onto the lyophobic surface with  $\theta_\delta = \pi$ . Similar behavior is found for bridges within a slab bounded by two structured surfaces [38]. Irrespective of the precise behavior of the contact line, the shape of the droplet will become more and more spherical in the limit of large  $V_\beta$ . This implies that the mean curvature  $M$  decays for large  $V_\beta$  and, thus, exhibits a maximum as a function of  $V_\beta$  for any shape of the domain boundary.

#### 4.2. Droplet Pattern on Several Surface Domains

The experimental procedures used to create structured or imprinted surfaces typically generate whole arrays or patterns consisting of many surface domains. Therefore, let us consider a surface pattern consisting of  $N$  identical surface domains, which are lyophilic with  $\theta_\gamma = 0$ , on an otherwise lyophobic surface with  $\theta_\delta = \pi$ . For simplicity, the domains are taken to be circular. We

now place a certain amount of  $\beta$  phase onto these circular domains and look for the wetting morphology of minimal free energy.

The droplets on the different surface domains must all have the same mean curvature  $M$  because of the Laplace equation  $2M\Sigma_{\alpha\beta} = P_\beta - P_\alpha$  as given by (3). For a spherical cap,  $M$  is simply the inverse of the radius of the sphere. In addition, the contact area of these droplets is fixed to be identical with the area of the circular surface domains (since we look at the limiting case with  $\theta_\gamma = 0$  and  $\theta_\delta = \pi$  and  $M > 0$ ). This implies that the ensemble of droplets can only consist of two different types of droplets: small ones with contact angle  $\theta_{sm}$  and large ones with contact angle  $\theta_{la}$ . If one combines a small droplet with a large one in such a way that they are pasted together along their flat contact areas, one obtains a complete sphere which implies  $\theta_{sm} + \theta_{la} = \pi$ .

One must now consider different arrangements consisting of  $N_{sm}$  small and  $N_{la}$  large droplets with  $N_{sm} + N_{la} = N$  as shown in Fig. 3. Somewhat surprisingly, a systematic calculation of the corresponding free energies shows that only two of these possible arrangements represent stable or metastable states [1]: (i) The homogeneous droplet pattern, denoted by (A), consisting of a chain of identical droplets see Fig. 3(a), and (ii) heterogeneous droplet patterns denoted by (B) consisting of only one large droplet and  $N - 1$  small ones as shown in Fig. 3(b). This pattern is  $N$ -fold degenerate since the large droplet can sit on any of the  $N$  domains. All other droplet patterns which contain two or more large droplets are saddle points in shape space and must eventually decay into the patterns (A) or (B).

The coexistence of the two morphologies (A) and (B) is intimately related to the fact that the mean curvature  $M$  of a single droplet exhibits a maximum as a function of the droplet volume. Since this latter

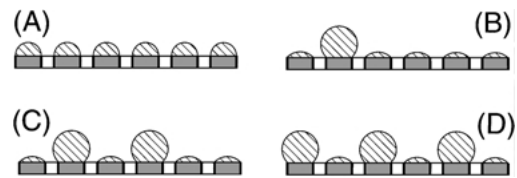


Figure 3. Possible droplet patterns on a lattice of circular domains. In each configuration, all droplets must have the same mean curvature which implies that the small and the large droplet form a complete sphere when pasted together along their flat contact area. Droplet patterns such as (C) and (D) that contain more than one large droplet are unstable and must decay either into the homogeneous pattern (A) or into the inhomogeneous pattern (B) with only one large droplet.

property holds for all surface domains as mentioned, the (A) and (B) morphologies should be present for any pattern of  $N$  domains with identical but *arbitrary* shape. The same type of transition occurs for contact angles  $\theta_\gamma > 0$  and  $\theta_\delta < \pi$  provided the wettability contrast is not too small.

The transition from the (A) to the (B) morphology can be understood intuitively if one considers the two limits in which the volume  $V_\beta$  is small and large, respectively. In the limit of small  $V_\beta$ , the  $\beta$  phase can maximize its contact with the  $N$  lyophilic  $\gamma$  domains without any constraint arising from the area of the  $\alpha\beta$  interface. Thus, for small  $V_\beta$ , the  $\beta$  phase will form identical small ‘pancakes’ on all  $\gamma$  domains. However, the total area of the droplet grows at least as  $\sim V_\beta^{2/3}$  and, thus, becomes large for large  $V_\beta$ . Therefore, as soon as  $V_\beta$  is large compared to  $V_\gamma$ , the  $\beta$  phase will prefer to form one large droplet in order to minimize the area of its  $\alpha\beta$  interface. Thus, the limits of small and large volume  $V_\beta$  lead to two different states, and one can anticipate a morphological transition at an intermediate value  $V_\beta = V_c$ .

#### 4.3. Channel Transitions

One example for a morphological wetting transition which has been studied in some detail is the transition of water channels on hydrophilic stripes as shown in Figs. 4 and 5. [2]. The two micrographs displayed in Fig. 4(a) and (b) show the state of the water channels before and after the transition, respectively. Inspection of this figure shows that each channel undergoes a transition from a state with uniform cross-section to a channel with a single bulge. These different states have also been calculated within the theoretical framework described above. Since the width of the lyophilic stripes is 30 micrometers, the line tension contributions to the free energy can be safely ignored. The bulge state was calculated by numerical minimization using (i) available packages such as the Surface Evolver [57] and (ii) a special code which was developed for the channel geometry. As shown in Fig. 5, the theoretical shapes agree rather well with the experimental observations.

In the experiments, the striped  $\gamma$  domains were created by thermal vapor deposition of  $\text{MgF}_2$  onto a hydrophobic silicone rubber or thiolated gold substrate through appropriate masks. The resulting hydrophilic  $\text{MgF}_2$  stripes have a width of  $30 \mu\text{m}$  and a contact angle  $\theta = \theta_\gamma$  of about 5 degrees for water. Both the silicone rubber and the thiolated gold had a contact angle  $\theta = \theta_\delta$

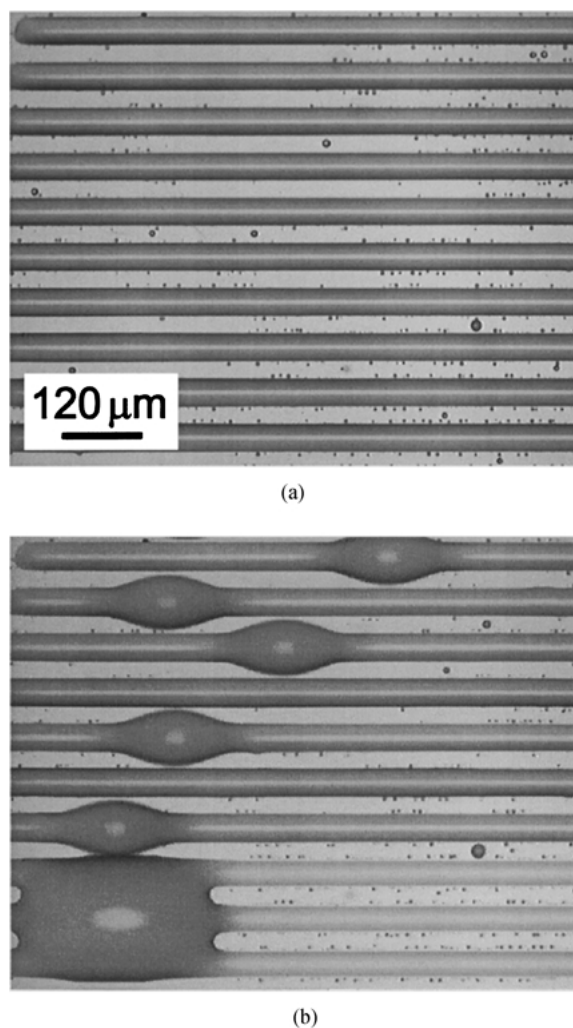


Figure 4. Channel transition of water channels on a striped surface. (a) If the amount of water per channel is below the critical volume, the channels are thin and homogeneous and their shape is given by cylindrical segments; (b) If the water volume exceeds the critical value, each channel develops a single bulge. The width of both the hydrophilic and the hydrophobic stripes is 30 micrometers.

of about 108 degrees. The projected shape of the channel was studied by optical microscopy, the shape of the contact line by surface plasmons. As shown in Fig. 5, the contact line is found to detach from the hydrophilic stripe and to make an excursion across the hydrophobic surface domain.

The theoretical shapes have been determined by minimization of the interfacial free energies of the water channel. Contributions from the contact line can be safely ignored since all linear dimensions of the water channel are in the micrometer regime. Therefore, the

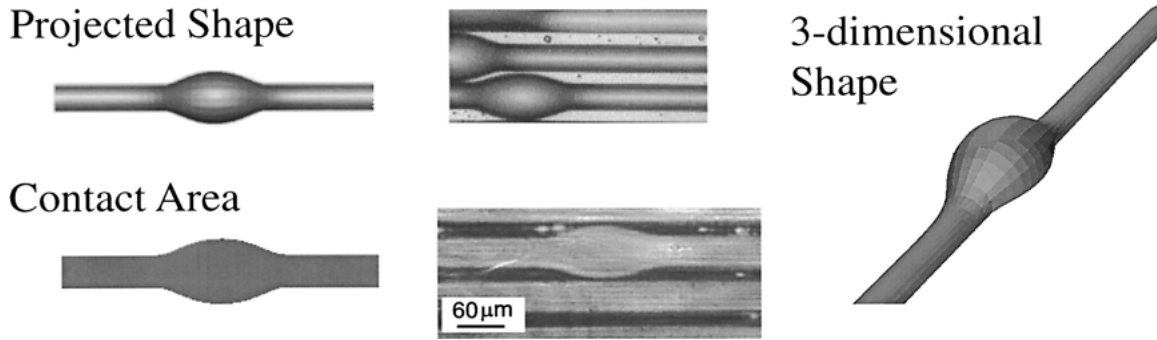


Figure 5. Channel state with a bulge: Comparison of theory (left and experiment (middle) for the projected shape of the channel and for the shape of the contact line. The drawing on the right shows the full 3-dimensional shape as determined theoretically.

only parameters which enter the calculation are the two contact angles  $\theta = \theta_\gamma$  and  $\theta = \theta_\delta$  of the hydrophilic and hydrophobic domains, the geometry of the surface domains, and the total volume  $V_\beta$  of water condensed onto these domains. Thus, the theory does not contain any fitting parameter. In contrast to the experimental observations, the theoretical calculations also provide the full 3-dimensional shape of the bulge state.

Morphological transitions from a channel with uniform cross-section to a channel with a single bulge also occur for ring-shaped surface domains consisting of an annulus with a constant width [5]. In this latter case, the appearance of the bulge *spontaneously* breaks the rotational symmetry of the ring channel which implies that the bulge position is degenerate. Therefore, angular displacements of this bulge do not cost any (free) energy, and the corresponding interface deformation represents a ‘soft mode’ which should be observable for domains in the micrometer regime.

As explained before, the wetting structures considered here are not subject to external body forces such as gravity which act directly on the sub-volumes of the  $\beta$  liquid. The latter forces accelerate the  $\beta$  liquid and may explicitly break the symmetry of the wetting geometry, see, e.g., [58]. In contrast, the morphological transitions described here lead to *spontaneous* symmetry breaking which is not related to an external force field.

#### 4.4. Bridges in Structured Slit Pores and Slabs

Another geometry which can be realized experimentally are slit pores and slabs bounded by structured surfaces [4, 19]. The first theoretical studies addressed sinusoidally structured substrates which were investi-

gated by Monte-Carlo simulations [53] and by variational methods [47]. These systems also exhibit morphological wetting transitions as first pointed out in [38].

The simplest pattern of surface domains consists of a single pair of opposing lyophilic stripes, see Fig. 6. The two surfaces are separated by  $L_\perp$ , the two  $\gamma$  stripes have width  $L_\gamma$ , lie parallel to each other but may be displaced by  $\Delta L$  as indicated in Fig. 6(c). If a certain amount of  $\beta$  phase is placed within such a structured slab, this liquid forms a bridge connecting the two stripes as long as the surface separation  $L_\perp$  is sufficiently small, see Fig. 6(a) and (b). For larger values of  $L_\perp$ , this bridge will break and form two separate channels as in Fig. 6(c).

If the striped surface domains are relatively long, one may ignore effects arising from their ends. In such a situation, the wetting morphologies are translationally invariant parallel to the stripes and are completely determined by their cross-section as shown in Fig. 6. However, if one takes the finite length of the surface stripes into account, one often finds bridges which are

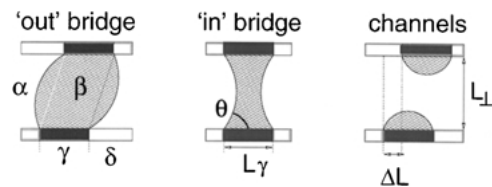


Figure 6. Different  $\beta$  phase morphologies within a slit pore or slab bounded by two structured surfaces which contain a lyophilic  $\gamma$  stripe: (left) ‘Out’ bridge with positive mean curvature; (middle) ‘In’ bridge with negative mean curvature; and (right) Broken bridge or 2-channel state. The width of the  $\gamma$  stripes is  $L_\gamma$ , the two surfaces have separation  $L_\perp$ , and the two stripes may be displaced laterally by  $\Delta L$ .

localized in space and, thus, are far from any translationally invariant state [39].

As one varies the surface separation  $L_{\perp}$  or the lateral displacement  $\Delta L$  for fixed volume of  $\beta$  phase, the bridge will deform and will then induce certain restoring forces. For  $\Delta L = 0$ , this restoring force acts perpendicular to the surfaces and can be calculated via  $K_{\perp} \equiv \delta \mathcal{F}_{\text{br}} / \delta L_{\perp}$  where  $\mathcal{F}_{\text{br}}$  is the free energy of the bridge state. The perpendicular force  $K_{\perp}$  vanishes for a certain separation  $L_{\perp} = L_{\perp 0}$  which corresponds to a minimum of the bridge free energy and to a characteristic contact angle  $\theta = \theta_0$  where  $\theta$  is defined in Fig. 6(b). This angle satisfies the simple relation [38]

$$\tan \theta_0 = -L_{\gamma} / L_{\perp} \quad \text{for} \quad \Delta L = 0. \quad (8)$$

Thus, if one of the two surfaces can move in response to the force arising from the liquid bridge, the contact angle will spontaneously assume the value  $\theta = \theta_0$ . This optimal bridge will be an ‘out’ bridge as in Fig. 6(a), since the relation (8) implies  $\pi/2 < \theta_0 < \pi$ .

In the case of many stripes on the two opposing surfaces of the slab, one has a whole sequence of morphological transitions at which more and more bridges break as one increases the surface separation  $L_{\perp}$  [38].

## 5. Summary and Outlook

In summary, structured surfaces which contain patterns of lyophilic surface domains generically lead to morphological wetting transitions. For a single surface, any pattern of lyophilic  $\gamma$  domains can be characterized by a reference volume  $V_{\gamma}$  corresponding to a unique constant mean curvature shape. The latter shape is defined by two properties: (i) The contact line is pinned to the  $\gamma\delta$  domain boundaries which implies that the contact area between the  $\beta$  phase and the substrate surface is equal to the  $\gamma$  domains; and (ii) The mean curvature attains its maximal value  $M = M_{\text{max}}$ . If a certain amount of  $\beta$  phase is deposited on such a surface, it will undergo a morphological wetting transition at a certain volume  $V_{\beta} = V_c$  which is of the same order of magnitude as  $V_{\gamma}$ .

For two structured surfaces bounding a slit pore or slab, the corresponding reference volume  $V_{\gamma}$  may be defined to be equal to the sum of the two reference volumes for the two surfaces. In this case, one has additional bridge states which exert forces on the two opposing surfaces. For a fixed amount of  $\beta$  phase, these

forces vanish for a characteristic separation of the two surfaces corresponding to a characteristic contact angle  $\theta = \theta_0$  of the bridges. For a single pair of opposing stripes, this contact angle is given by (8).

The morphological transitions discussed here occur for a wide range of domain sizes  $L_{\gamma}$  from the millimeter to the nanometer regime. For intermediate domain sizes between the capillary length  $L_{\text{cap}}$ , which is of the order of millimeters, and the characteristic length scale  $|\Delta| / \Sigma_{\alpha\beta}$ , which is typically tens of nanometers, the morphology of the wetting layer is primarily determined by the different interfacial tensions or the corresponding contact angles. The various examples which have been discussed explicitly in Section 4 belong to this intermediate size regime.

It is straightforward to extend these calculations to domain sizes, which are large compared to the capillary length  $L_{\text{cap}}$ . One then has to include gravity which acts as a body force and will flatten and/or distort the wetting morphologies depending on the orientation of the substrate surface. Likewise, one may study very thin wetting layers which experience a body potential arising from the molecular interactions with the structured substrate.

In this article, I have focussed on the situation in which the  $\beta$  phase is a liquid and the  $\alpha$  phase is a vapor or another liquid. However, morphological wetting transitions also occur if the wetting phase  $\beta$  is a solid. In this case, the  $\alpha\beta$  interface has an anisotropic tension and may be affected by elastic strains. Thus, the corresponding shapes are more difficult to calculate but this does not change the presence and the overall character of the transition. One model system for which such transitions have been explicitly determined is the simple cubic lattice gas which is also known as the Kossel crystal. [59] Another process which involves morphological wetting transitions is surface melting adjacent to a structured substrate.

Finally, wetting of structured surfaces also leads to interesting time-dependent phenomena as studied in [60–62] and is relevant for many applications such as microreactors [3, 63] and microfluidics [13, 64, 65].

## Acknowledgments

It is a pleasure to thank Martin Brinkmann, Willi Fenzl, Hartmut Gau, Stephan Herminghaus, Peter Lenz, Peter Swain, and Antonia Valencia for stimulating interactions and fruitful collaborations.

## References

1. P. Lenz and R. Lipowsky, Phys. Rev. Lett. **80**, 1920 (1998).
2. H. Gau, S. Herminghaus, P. Lenz, and R. Lipowsky, Science **283**, 46 (1999).
3. R. Lipowsky, P. Lenz, and P. Swain, Colloids and Surfaces A **161**, 3 (2000).
4. J. Silver, Z.H. Mi, K. Takamoto, P. Bungay, J. Brown, and A. Powell, J. Coll. Interface Sci. **219**, 81 (1999).
5. P. Lenz, W. Fenzl, and R. Lipowsky, Europhys. Lett., **53**, 618 (2001).
6. G. López, H. Biebuyck, C. Frisbie, and G. Whitesides, Science **260**, 647 (1993).
7. J. Drelich, J.D. Miller, A. Kumar, and G.M. Whitesides, Colloids and Surfaces A **93**, 1 (1994).
8. F. Morhard, J. Schumacher, A. Lenenbach, T. Wilhelm, R. Dohint, M. Grenze, and D.S. Everhart, Electrochem. Soc. Proc. **97**, 1058 (1997).
9. E. Meyer and H. Braun, Macromol. Materials Eng. **276**, 44 (2000).
10. S. Herminghaus, A. Fery, and D. Reim, Ultramicroscopy **69**, 211 (1997).
11. G. Möller, M. Harke, and H. Motschmann, Langmuir **14**, 4955 (1998).
12. R. Wang, A.N. Parikh, J.D. Beers, A.P. Shreve, and B. Swanson, J. Phys. Chem. B **103**, 10149 (1999).
13. M. Gleiche, L. Chi, and H. Fuchs, Nature **403**, 173 (2000).
14. R. Hayward, D. Saville, and I. Aksay, Nature **404**, 56 (2000).
15. A. Higgins and R. Jones, Nature **404**, 476 (2000).
16. F. Burmeister, C. Schäfle, T. Matthes, M. Böhmisch, J. Boneberg, and P. Leiderer, Langmuir **13**, 2983 (1997).
17. U. Drodofsky, J. Stuhler, T. schulze, M. Drewsen, B. Brezger, T. Pfau, and J. Mlynek, Appl. Phys. B **65**, 755 (1997).
18. J. Heier, E.J. Kramer, S. Walheim, and G. Krausch, Macromolecules **30**, 6610 (1997).
19. R. Garcia, M. Calleja, and F. Perez-Murano, Appl. Phys. Lett. **72**, 2295 (1998).
20. R. Finn, *Equilibrium Capillary Surfaces* (Springer, New York, 1986).
21. J. Rowlinson and B. Widom, *Molecular Theory of Capillarity* (Clarendon Press, Oxford, 1982).
22. P. Swain and R. Lipowsky, Langmuir **14**, 6772 (1998).
23. L. Boruvka and A. Neumann, J. Chem. Phys. **66**, 5464 (1977).
24. A.I. Rusanov, Colloid J. USSR (Engl. Transl.) **39**, 618 (1977).
25. A. Marmur, Colloids and Surf. A: Physiochem. Eng. Aspects **136**, 81 (1998).
26. S. Hildebrandt and A. Tromba, *Kugel, Kreis und Seifenblasen* (Birkhäuser Verlag, Basel, 1996).
27. H. Wente, Pacific J. Math. **189**, 339 (1999).
28. H. Wente, Math. Z. **120**, 277 (1971).
29. K. Steffen, Arch. Rat. Mech. Anal. **94**, 101 (1986).
30. M. Struwe, *Plateau's Problem and the Calculus of Variations* (Princeton University Press, Princeton, New Jersey, 1988).
31. J. Sullivan and F. Morgan, Int. J. Math. **7**, 833 (1996).
32. M. Struwe, *Variational Methods* (Springer Verlag, Berlin, 1996).
33. J. Gaydos and A.W. Neumann, in *Applied Surface Thermodynamics*, edited by A.W. Neumann and J.K. Spelt (Marcel Dekker, New York, 1996), p. 169.
34. D. Li, Colloids and Surfaces A **116**, 1 (1996).
35. J. Drelich, Colloids and Surfaces A **116**, 43 (1996).
36. T. Pompe, A. Fery, and S. Herminghaus, Langmuir **14**, 2585 (1998).
37. P. Lenz and R. Lipowsky, Eur. Phys. J. E **1**, 249 (2000).
38. P. Swain and R. Lipowsky, Europhys. Lett. **49**, 203 (2000).
39. A. Valencia, M. Brinkmann, and R. Lipowsky, Langmuir, (in press).
40. B. Derjaguin, N. Churaev, and V. Muller, *Surfaces Forces* (Consultants Bureau, New York, 1987).
41. R. Lipowsky, D. Kroll, and R. Zia, Phys. Rev. B **27**, 4499 (1983).
42. E. Brézin, B. Halperin, and S. Leibler, J. Physique **44**, 775 (1983).
43. R. Lipowsky, Phys. Rev. Lett. **52**, 1429 (1984).
44. R. Lipowsky, Phys. Rev. B **32**, 1731 (1985).
45. R. Lipowsky and M.E. Fisher, Phys. Rev. B **36**, 2126 (1987).
46. W. Koch, S. Dietrich, and M. Napiorkowski, Phys. Rev. E **51**, 3300 (1995).
47. P. Röcken, A. Somoza, P. Tarazona, and G. Findenegg, J. Chem. Phys. **108**, 8689 (1998).
48. J.R. Henderson, J. Phys. Condens. Matter **11**, 629 (1999).
49. C. Bauer, S. Dietrich, and A. Parry, Europhys. Lett. **47**, 474 (1999).
50. L. Frink and A. Salinger, J. Chem. Phys. **110**, 5969 (1999).
51. K. Rejmer and M. Napiorkowski, Phys. Rev. E **62**, 588 (2000).
52. M. Schoen and H. Bock, J. Phys. Cond. Matter **12**, A333 (2000).
53. M. Schön and D.J. Diestler, Chem. Phys. Lett. **270**, 339 (1997).
54. H. Bock and M. Schoen, J. Phys. Cond. Matter **12**, 1569 (2000).
55. A. Cassie, Discuss. Faraday Soc. **3**, 11 (1948).
56. J. Henderson, Molecular Phys. **98**, 677 (2000).
57. K. Brakke, Experimental Mathematics **1**, 141 (1990).
58. F. Zayas, J.I.D. Alexander, J. Meseguer, and J.F. Ramus, Phys. Fluids **12**, 979 (2000).
59. A. Valencia and R. Lipowsky, in preparation.
60. C. Schäfle, C. Bachinger, B. Rinn, C. David, and P. Leiderer, Phys. Rev. Lett. **83**, 5302 (1999).
61. R. Burghaus, Europ. Phys. J. E, in press.
62. R. Konnur, K. Kargupta, and A. Sharma, Phys. Rev. Lett. **84**, 931 (2000).
63. S. DeWitt, Curr. Opinion in Chem. Biol. **3**, 350 (1999).
64. M. Grunze, Science **283**, 41 (1999).
65. R. Schasfoort, S. Schlautmann, J. Hendrikse, and A. van den Berg, Science **286**, 942 (1999).